Starlight beneath the waves : in search of TeV photon emission from Gamma-Ray Bursts with the ANTARES Neutrino Telescope

Laksmana-Astraatmadja, T.

3 *Muon production in the atmosphere*

HIGH-ENERGY γ-rays produce muons when they interact with the Earth's atmosphere. These muons will then traverse down to the bottom of the sea, producing Čerenkov light that can be detected by the detector array. This idea of detecting γ-induced showers by detecting the produced muons has been around for a long time. However, early calculations performed in the 1960s seem to indicate that γ-induced showers are muon-poor, having only less than 10% the muon content of proton-induced showers (Stanev, Gaisser & Halzen, 1985). These calculations are contradicted when muons were firmly detected at underground detectors, coming from the direction of Cygnus X-3 (e.g. Marshak et al. 1985). Despite the low rates and weak signals, these detections raised the interest to build large-area detectors that can detect high-energy muons and thus operate as γ-ray observatory. Stanev, Vankov & Halzen (1985) then identify two channels in which muons can be produced in γ showers: photoproduction and direct muon-pair production. In photoproduction, muons are produced from the (semi)leptonic decay of pions or kaons produced by the interaction of high-energy photons with the atomic nucleus of the atmosphere. This is the most important channel to produce muons in the GeV regime. In direct muon-pair production, muons are created directly via the channel $\gamma + Z \rightarrow Z + \mu^+ + \mu^-$, in which Z is a nucleus of the atmosphere. Whereas muon production through photoproduction dies away with increasing energy, the cross section for muon-pair production increases with energy and thus muon-pair production is the dominant muon producing channel in the TeV regime.

In the following subsections we will describe the necessary formulation to calculate the muon flux generated in gamma-induced showers. For convenience, all units of length are converted into radiation lengths in the air λ_{rad}, which is taken to be 37.1 g cm^{-2}.

3.1 *The cascade equation: Approximation A*

HIGH-ENERGY photons interact with atoms in the atmosphere and initiate electromagnetic showers of particles that will cascade on their way through the atmosphere. Through materialization or Compton collision, pairs of electron-positron will be produced, which in turn emit additional photons by way of bremsstrahlung. At each step the number of particles increases but their average energy decreases (Rossi & Greisen, 1941). Nevertheless these secondary photons can also produce muons that can be detected by the detector array, and thus it is important to calculate the total number of photons produced in such a photon shower.

This problem of counting particles produced in electromagnetic showers can be solved if we consider only radiation phenomena and electron-pair production, which can be described by the asymptotic formula for complete screening. This solution is called Approximation A (Rossi & Greisen, 1941) and allows us to calculate the photon flux at some depth t in the atmosphere, given the initial photon energy spectrum. If the initial spectrum is in the form of a power law such as $\gamma(\epsilon) \propto \epsilon^{-(b+1)}$, then the resulting spectrum at depth t is (Rossi & Greisen 1941; Halzen, Kappes & Ó Murchadha 2009)

$$\gamma(\epsilon, t) = \gamma(\epsilon, t=0)\frac{(\sigma_0+\lambda_1)(\sigma_0+\lambda_2)}{\lambda_2-\lambda_1} \times \left[\frac{\exp(\lambda_1 t)}{\sigma_0+\lambda_1} - \frac{\exp(\lambda_2 t)}{\sigma_0+\lambda_2}\right] \tag{3.1}$$

In this Equation as well as the in the following calculations, t is the slant depth in units of radiation length (in the atmosphere, 1 radiation length equals 36.62 g cm^{-2}), $\sigma_0 = 7/9$ is the probability per radiation length that an electron pair production will take place (in a case of complete screening), and $\lambda_{1,2}$ are the scale lengths factor of the shower growth and dissipation in the atmosphere. The formula to calculate $\lambda_{1,2}$ as a function of spectral index b, as well as its tabulation, is given in Rossi & Greisen (1941). For $b < 1$, λ_1 is positive while for $b > 1$, λ_1 is negative. This would mean that in the former case the shower would grow as it penetrates the atmosphere while in the latter it will dissipate. Thus for a general case of an arbitrary value of b, the photon flux

can be decomposed into its spectrum at the top of the atmosphere and its scale factor at depth t, i.e

$$\gamma(\epsilon, t) = \gamma_0(\epsilon)\gamma_2(t). \tag{3.2}$$

Particularly important is the case for $b = 1$ since $\lambda_1 = 0$ and $\lambda_2 < 0$, and this would make the second exponential term in Equation 3.1 essentially zero after several radiation length, making the photon spectrum independent of depth:

$$\gamma(\epsilon_\gamma, t) = 0.567\gamma(\epsilon_\gamma, t = 0), \tag{3.3}$$

where the photon spectrum at the top of the atmosphere $\gamma(\epsilon_\gamma, t = 0)$ is as described in Equation 2.62.

3.2 *Pion decay*

THE INTERACTION of high-energy photons with atomic nuclei in the atmosphere can produce pions through the reaction $\gamma + N \rightarrow \pi + X$ followed by leptonic decay of pions into a positive muon and a muon neutrino, or a negative muon and a muon antineutrino:

$$\pi^\pm \rightarrow \mu^\pm + \nu_\mu(\overline{\nu}_\mu), \tag{3.4}$$

with a probabilty of close to 100% to occur. The formulation to calculate the muon spectrum from this channel has been calculated using the linear cascade equation and assuming a power-law photon spectrum with spectral index $b = 1$ by Drees, Halzen & Hikasa (1989), and its generalisation to an arbitrary spectral index by Halzen, Kappes & Ó Murchadha (2009).

For the case of $b \neq 1$, this paper will closely follow that of Halzen, Kappes & Ó Murchadha (2009), which begins by an ansatz that the differential pion spectrum in the atmosphere can be factorized as

$$\pi(\epsilon, t) = \gamma(\epsilon, t = 0)\pi_2(\epsilon, t), \tag{3.5}$$

in which $\pi_2(\epsilon, t)$ can be split in two regimes: the high energy regime where pion interactions dominate over decay, and the low

energy regime where pion interactions are neglected. The pion spectrum at high energy is

$$\pi_2^{\mathrm{HE}}(t) = \left[\frac{\exp(\lambda_1 t) - \exp(-t/\Lambda_\pi)}{(\sigma_0 + \lambda_1)(\lambda_1 + \frac{1}{\Lambda_\pi})} - \frac{\exp(\lambda_2 t) - \exp(-t/\Lambda_\pi)}{(\sigma_0 + \lambda_2)(\lambda_2 + \frac{1}{\Lambda_\pi})} \right] \times \frac{z_{\gamma\pi}}{\lambda_{\gamma A}} \frac{(\sigma_0 + \lambda_1)(\sigma_0 + \lambda_2)}{\lambda_2 - \lambda_1}, \tag{3.6}$$

while the spectrum at low energy is

$$\pi_2^{\mathrm{LE}}(\epsilon, t) = \frac{z_{\gamma\pi}}{\lambda_{\gamma A}} \frac{(\sigma_0 + \lambda_1)(\sigma_0 + \lambda_2)}{\lambda_2 - \lambda_1} \times \int_0^t dt' \left(\frac{t'}{t}\right)^\delta \left[\frac{\exp(\lambda_1 t')}{\sigma_0 + \lambda_1} - \frac{\exp(\lambda_2 t')}{\sigma_0 + \lambda_2} \right], \tag{3.7}$$

in which $\delta = t/d_\pi$, where d_π is the decay length

$$d_\pi = \frac{\epsilon t \cos\theta}{\epsilon_\pi}, \tag{3.8}$$

here $\epsilon_\pi = 115$ GeV is the pion decay energy constant.

The integral in Equation 3.7 can be expanded into series:

$$\int_0^t dt' \left(\frac{t'}{t}\right)^\delta \frac{\exp(\lambda_i t')}{\sigma_0 + \lambda_i} \approx \frac{1}{\sigma_0 + \lambda_i} \sum_{j=1}^{100} \frac{\lambda_i^{j-1} t^j}{(j-1)!(\delta + j)}. \tag{3.9}$$

In Equation 3.6 and 3.7,

$$\Lambda_\pi = 173 \text{ g cm}^{-2} = 4.66 \text{ radiation lengths} \tag{3.10}$$

is the effective pion interaction length in the atmosphere,

$$z_{\gamma\pi} = \frac{\sigma_{\pi\pi}}{\sigma_{\gamma N}} = \frac{2}{3} \tag{3.11}$$

is the ratio between cross sections $\sigma_{\gamma\to\pi}$ and $\sigma_{\gamma N}$, and

$$\lambda_{\gamma A} = 446.14 \text{ radiation lengths} \tag{3.12}$$

is the interaction length of photons in atmospheric nuclei. These values are assumed to vary little for different spectral indices and energy.

Due to the unavailability of an analytical expression for both energy regime, taking a smooth transition from one regime to another is difficult. The pion spectrum at all energy regime is then

$$\pi(\epsilon, t) = \gamma(\epsilon, t = 0) \min\left[\pi_2^{\mathrm{HE}}(t), \pi_2^{\mathrm{LE}}(\epsilon, t)\right]. \tag{3.13}$$

The muon flux at the surface of the Earth can then be obtained by using standard 2-body decay kinematics, assuming no muon decay and energy loss in the atmosphere:

$$\frac{dN_\mu}{d\epsilon_\mu} = \int_0^{t_{\max}} dt B_{\mu\pi} \int_\epsilon^{\epsilon/r} \frac{d\epsilon'}{(1-r)\epsilon'} \frac{\pi(\epsilon', t)}{d_\pi(t)}, \tag{3.14}$$

in which $r = (m_\mu/m_\pi)^2$ and $B_{\mu\pi} = 1$ is the number of muons produced for each decaying pion. The maximum depth $t_{\max}$ is determined using

$$t_{\max} = \lambda_{e^+e^-} \ln\left[\frac{\epsilon_{\max}\langle x\rangle_{\gamma\to\mu}}{\epsilon}\right], \tag{3.15}$$

where $\lambda_{e^+e^-} = 9/7$ is the electromagnetic cascade length and $\langle x\rangle_{\gamma\to\mu} = 0.25$ is the fraction of γ-ray energy that goes into the final muon for the case of pion decays.

For the special case of $b = 1$, we calculate the muon spectrum using the formulation by Drees, Halzen & Hikasa (1989):

$$\frac{dN_\mu}{d\epsilon_\mu} = \gamma(\epsilon_\mu, t = 0) \frac{\Lambda_\pi}{\lambda_{\gamma A}} z_{\gamma\pi} \frac{L_\gamma}{1 + (L_\gamma/H_\gamma)\epsilon_\mu\epsilon_\pi\cos\theta}, \tag{3.16}$$

where

$$L_\gamma = \frac{1-r^2}{2(1-r)} \frac{t_{\max}}{\Lambda_\pi}, \quad H_\gamma = \frac{1-r^3}{3(1-r)}\left[1 + \ln\frac{t_{\max}}{\Lambda_\pi}\right]. \tag{3.17}$$

The constant terms $(\Lambda_\pi, z_{\gamma\pi}, \lambda_{\gamma A})$ in the Equations above are the same as in Equations 3.10–3.12

3.3 *Direct muon-pair production*

THE FEYNMAN diagram for direct lepton-pair production $\gamma + N \to N + l^+ + l^-$ is pictured in Figure 3.1. This reaction occurs when an impacting photon interacts with a photon within the

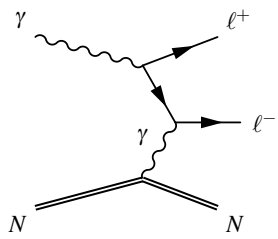

Figure 3.1: Feynman diagram for lepton-pair production in the presence of a nucleus N

electric field of a nucleus, producing a pair of leptons. The second photon is necessary to maintain the conservation of 4-momentum, transferring the required momentum from the nucleus. Lepton-pair production is related to bremsstrahlung by a substitution rule and the calculation of the cross section can be done if we know how to calculate bremsstrahlung by electrons (Tsai, 1974). For the interaction of a photon with nuclear electrons to produce muon-pair, the photon energy threshold must then be

$$\epsilon_{\text{th}} = \frac{2m_\mu}{m_e}\left(m_\mu + m_e\right) \simeq 43.9\,\text{GeV}, \tag{3.18}$$

where m_e is the electron mass and m_μ is the muon mass.

To calculate an approximate formula of muon-pair production, what is usually done is taking the Bethe-Heitler result for electron-pair production (Bethe & Heitler, 1934) and substitute the electron mass with that of muon. This generalization would not be correct, however, because the atomic form factor involved in the calculation must be integrated over the transferred momentum in which the upper limit is approximately the mass of the lepton involved (Halzen, Kappes & Ó Murchadha, 2009).

We will now discuss the necessary calculations to obtain the accurate formula for the cross section of muon-pair production.

The impacting photon energy will be fully shared by the resulting muon-pair according to

$$\epsilon_\gamma = \epsilon_\mu^+ + \epsilon_\mu^-, \tag{3.19}$$

or in terms of fraction of photon energy:

$$x_+ = \frac{\epsilon_\mu^+}{\epsilon_\gamma}, \quad x_- = \frac{\epsilon_\mu^-}{\epsilon_\gamma}, \quad x_+ + x_- = 1. \tag{3.20}$$

To take into account the atomic and nuclear form factors, we need the differential cross section equation as a function of the momentum transfer. Since this work concerns very high-energy photons, we can use the ultrarelativistic approximation written as (Bethe & Heitler, 1934)

$$\frac{d\sigma}{dx_+} = 4\alpha Z^2\left(r_0\frac{m_e}{m_\mu}\right)^2\left[\left(x_+^2 + x_-^2\right)\Phi_1(\delta) + \frac{2}{3}x_+x_-\Phi_2(\delta)\right],$$

(3.21)

where α is the fine-structure constant, Z is the charge of the nucleus—for the Earth's atmosphere $Z = 7.37$ (Rossi, 1952), r_0 is the classical electron radius, and δ is the screening parameter equal to the necessary minimum momentum transfer from the nucleus:

$$\delta \simeq q_{\min} = \frac{m_\mu^2}{2\epsilon_\gamma x_+ x_-}. \tag{3.22}$$

The functions $\Phi_{1,2}$ are integrals of form factors over transferred momentum q. Whereas electron-pair production involves only the atomic form factors, in the case of muon-pair production it is also necessary to consider the nuclear form factors since the momentum involved is much larger than the inverse square of the atomic radius (Tsai, 1974). The functions $\Phi_{1,2}$ would then be

$$\Phi_{1,2}(\delta) = \int_\delta^{q_{\max}} \frac{dq}{q^3} \left[F_n(q) - F_a(q)\right]^2 \psi_{1,2}(q,\delta), \tag{3.23}$$

where F_n and F_a are respectively the nuclear and atomic form factors and $\psi_{1,2}$ are the wave functions of the nucleus.

Equation 3.23 has been solved with several assumptions. We take the solution of Kelner, Kokoulin & Petrukhin (1995) in which a single function $\Phi(\delta) = \Phi_1 = \Phi_2$ is used for the case of complete screening. By taking the effects of complete screening into account we consider the fact that atoms are essentially neutral at large distance. This is because the electric charge of the nucleus get "screened" by the atomic electrons, i.e. their field are canceled by opposite electric charge of the atomic electrons, reducing the effective charge according to distance and thus limiting the maximum distance at which photons can still interact.

The contribution from inelastic form factors is also considered. This must also be taken into account since muon bremsstrahlung occurs on electrons bound in the atom and not on free electrons (Kelner, Kokoulin & Petrukhin, 1995).

Having considered both elastic and inelastic form factors, Equation 3.21 then becomes

$$\frac{d\sigma}{dx}(x,\epsilon_\gamma) = 4\alpha Z^2 \left(r_0 \frac{m_e}{m_\mu}\right)^2 \left[1 - \frac{4}{3}x(1-x)\right] \left[\Phi_{\text{el}}(\delta) + \frac{1}{Z}\Phi_{\text{in}}(\delta)\right].$$

(3.24)

The elastic contribution $\Phi_{\rm el}(\delta)$ is in the form of

$$\Phi_{\rm el}(\delta) = \ln\left[\Phi_\infty \frac{1+(D_n e^{1/2}-2)\delta/m_\mu}{1+BZ^{-1/3}e^{1/2}\delta/m_e}\right], \tag{3.25}$$

where

$$\Phi_\infty = \frac{BZ^{-1/3}}{D_n}\frac{m_\mu}{m_e}, \quad \delta = \frac{m_\mu^2}{2\epsilon_\gamma x(1-x)}, \quad e^{1/2} = 1.6187\ldots$$

$$\begin{array}{lll} B = 202.4 & D_n = 1.49 & \text{for Hydrogen, and} \\ B = 183 & D_n = 1.54A^{0.27} & \text{otherwise.} \end{array} \tag{3.26}$$

Here A is the atomic number of the nuclei involved. For our case of the Earth's atmosphere, $A = 14.78$ (Rossi, 1952).

The inelastic contribution $\Phi_{\rm in}(\delta)$ is

$$\Phi_{\rm in} = \ln\left[\frac{m_\mu/\delta}{m_\mu\delta/m_e^2 + e^{1/2}}\right] - \ln\left[1+\frac{1}{B'Z^{-2/3}e^{1/2}\delta/m_e}\right], \tag{3.27}$$

where $B' = 1429$. We can see that the differential cross section is symmetric in x_+ and x_-, thus we can write

$$x_+x_- = x - x^2,$$

where x substitutes either x_+ or x_- and the other becomes $(1-x)$.

In Figure 3.2 Equation 3.24 for various values of photon energy ϵ_γ is shown. We can see that due to the "screening" effect the cross section does not increase indefinitely but saturates as ϵ_γ increases. I integrate the differential cross section over x to obtain the total cross section as a function of photon energy and the result is shown in Figure 3.3. In the figure it is shown that saturation of the cross section occurs when the impacting photon energy $\epsilon_\gamma \approx 10$ TeV.

Using the cascade equation, we can calculate the muon-pair flux at sea level:

$$\frac{dN_\mu}{d\epsilon_\mu} = 2\lambda_{\rm rad}\frac{N_A}{A}\gamma_0\left(\epsilon_\mu\right)\int_0^1 dx x^b \frac{d\sigma}{dx}\left(x, \frac{\epsilon_\mu}{x}\right)\int_0^{t_{\rm max}} dt\gamma_2(t,b), \tag{3.28}$$

where N_A is the Avogadro number.

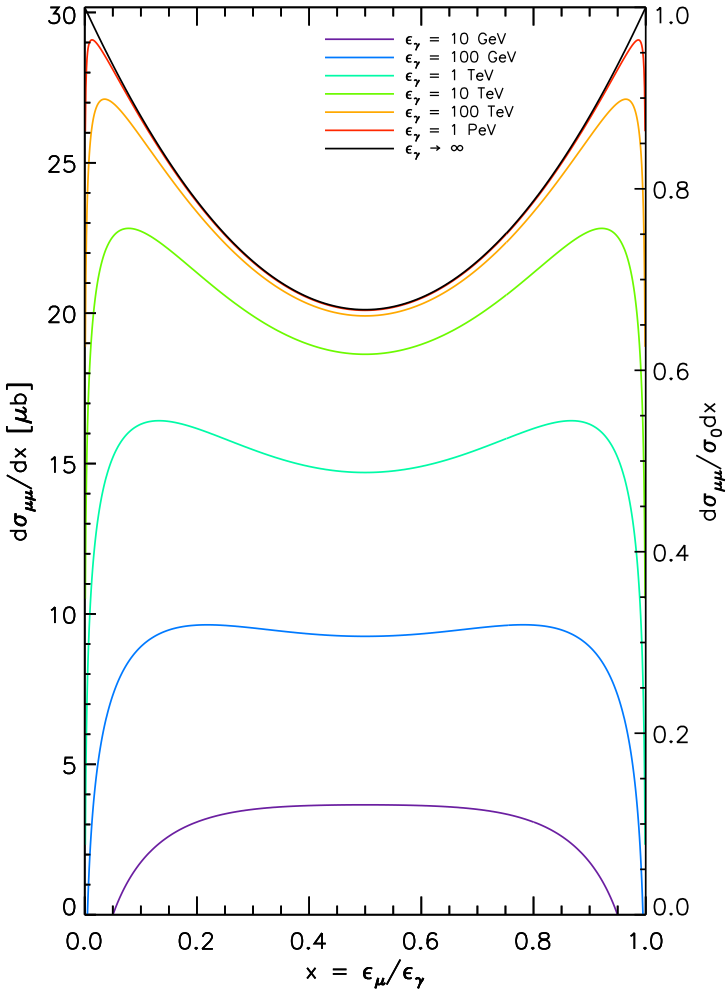

Figure 3.2: Differential cross section of muon-pair production (Equation 3.24) in the Earth's atmosphere for various values of impacting photon energy ϵ_γ, as a function of $x = \epsilon_\mu/\epsilon_\gamma$ which is the ratio between the resulting muon energy and the photon energy. The atomic and mass number of the atmosphere is taken to be $(A, Z) = (14.78, 7.37)$.

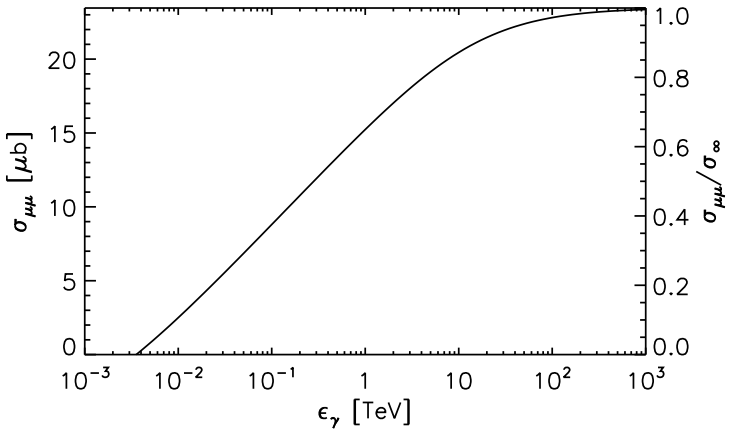

Figure 3.3: Total cross section of the process $\gamma \to \mu^+\mu^-$ in the Earth's atmosphere as a function of impacting photon energy ϵ_γ. Due to screening effect which limits the maximum distance in which high-energy photons can still interact with the nucleus, the cross section saturates for impacting photon energy $\epsilon_\gamma \gtrsim 10$ TeV.

3.4 Other channels of muon production

A γ-SHOWER can also produce kaons and the hadronic decay of kaons can produce a positive muon and a muon neutrino or a negative muon and a muon antineutrino:

$$K^\pm \to \mu^\pm + \nu_\mu(\overline{\nu}_\mu). \tag{3.29}$$

This reaction has only ∼63.5% chance of occuring (Gaisser, 1990). Furthermore, results from Halzen, Kappes & Ó Murchadha (2009) showed that the muon yield from kaon decays and other channels involving kaons can be neglected.

Positrons produced in γ-showers can also produce pairs of muon by interaction with an atomic electron through reaction $e^+e^- \to \mu^+ + \mu^-$. However, cross section for this reaction is very small and peaked at ∼61 GeV and falls rapidly with energy and is essentially zero for $\epsilon_\mu \gtrsim 700$ GeV (Halzen, Kappes & Ó Murchadha, 2009). Thus this production channel can also be neglected altogether.

3.5 Cosmic ray-induced muon background

IN ORDER to calculate the detection significance of photon-induced muons, we need to know the amount of the background in our observation. In our case of photon-induced muons detection, the

background consists of cosmic-ray induced muons. These muons are produced mainly through leptonic decay of pions, which is essentially the same channel discussed in Section 3.2. Leptonic decay of Kaons is also another channel of muon production albeit it is less important.

The energy spectrum of cosmic-ray induced muons, as a function energy and zenith distance, has already been parametrized by Gaisser (1990) as

$$\frac{dN_\mu}{d\epsilon_\mu} \approx 0.14\epsilon_\mu^{-2.7}\left[\frac{1}{1+\frac{1.1\epsilon_\mu\cos\theta}{115\text{GeV}}} + \frac{0.054}{1+\frac{1.1\epsilon_\mu\cos\theta}{850\text{GeV}}}\right] \text{GeV}^{-1}\ \text{cm}^{-2}\ \text{s}^{-1}\ \text{sr}^{-1}. \tag{3.30}$$

This parametrization overestimates the actual measured muon flux for energies below 10 GeV because at that energy regime muon decay and muon energy loss become important factors (see Figure 6.1 in Gaisser 1990). However, this will not be our concern since this is far below the energy regime we are interested in, and Equation 3.30 fits perfectly well for high-energy regime. This equation estimates the muon flux at sea level, thus if we want to estimate the muon background at detector we have to apply the appropriate muon energy loss formula for seawater. We will discuss this later in Section 3.6.

3.6 *Passage of muons through seawater*

Upon traversing a medium, energetic muons lose their energy through ionization and radiative processes. This energy loss can be treated by taking the standard formula to calculate the average energy loss (Barrett et al., 1952)

$$-\frac{d\epsilon}{dx} = a(\epsilon) + b(\epsilon)\epsilon, \tag{3.31}$$

in which $a(\epsilon)$ is the ionization contribution of the energy loss, while $b(\epsilon) = b_p(\epsilon) + b_b(\epsilon) + b_n(\epsilon)$ is the radiative contribution consisting of e^+e^- pair production (b_p), bremsstrahlung (b_b), and photonuclear interaction b_n.

Here I take the approach of Klimushin, Bugaev & Sokalski (2001) by splitting $a(\epsilon)$ into two separate processes, $a(\epsilon) = a_c(\epsilon) + a_e(\epsilon)$, where a_c is the classical ionization process sufficiently described by the "Bethe" equation (Nakamura & Particle Data Group, 2010) and a_e is the e diagrams for bremsstrahlung treated as part of an ionization process. a_c can thus approximated by

$$a_c(\epsilon) = a_{c_0} + a_{c_1} \ln\left(\frac{W_{\max}}{m_\mu}\right), \quad W_{\max} = \frac{\epsilon}{1 + \frac{m_\mu^2}{2m_e\epsilon}}, \tag{3.32}$$

in which $W_{\max}$ is the maximum transferable energy to the electron and $m_{\mu,e}$ are respectively the masses of muon and electron. The coefficients, in units of (10^{-6} TeV cm^2 g^{-1}), are $(a_{c_0}, a_{c_1}) = (2.106, 0.0950)$ for $\epsilon \leq 45$ GeV and $(a_{c_0}, a_{c_1}) = (2.163, 0.0853)$ for $\epsilon > 45$ GeV. For a_e, a polynomial approximation is used:

$$\begin{aligned} a_e(\epsilon) = {} & 3.54 + 3.785 \ln\epsilon + 1.15 \ln^2\epsilon \\ & + 0.0615 \ln^3\epsilon \quad 10^{-9} \text{ TeV cm}^2 \text{ g}^{-1}, \end{aligned} \tag{3.33}$$

where ϵ is in units of GeV.

The terms of b are parametrized in a polynomial function in the form

$$b_i(\epsilon) = \sum_{j=0}^{4} b_{ij} \ln^j \epsilon, \quad \text{where } i = p, b, n. \tag{3.34}$$

Here the energy input ϵ is also in units of GeV. The values of coefficients for b_{ij} is already calculated by Klimushin, Bugaev & Sokalski (2001) and is tabulated in their Table II. These formulations of energy loss are expected to still valid for $\epsilon_{\text{detector}} = 30$ GeV $- 5$ TeV and slant depth $(3 - 12)$ km with errors up to $\pm(6 - 8)\%$ (Klimushin, Bugaev & Sokalski, 2001).

Taking into account these contributions, the total muon energy loss in seawater as a function of energy is shown in Figure 3.4. In this figure we can see that at high energies radiative processes are more important than ionization. The critical energy at which the energy loss from ionization and radiative processes are equal can be calculated by solving $\epsilon_{\mu c} = a(\epsilon_{\mu c})/b(\epsilon_{\mu c})$. In the case of seawater this is $\epsilon_{\mu c} \sim 590$ GeV. Below this critical energy the dominant process is ionization while above this limit the radiative processes starts to dominate.

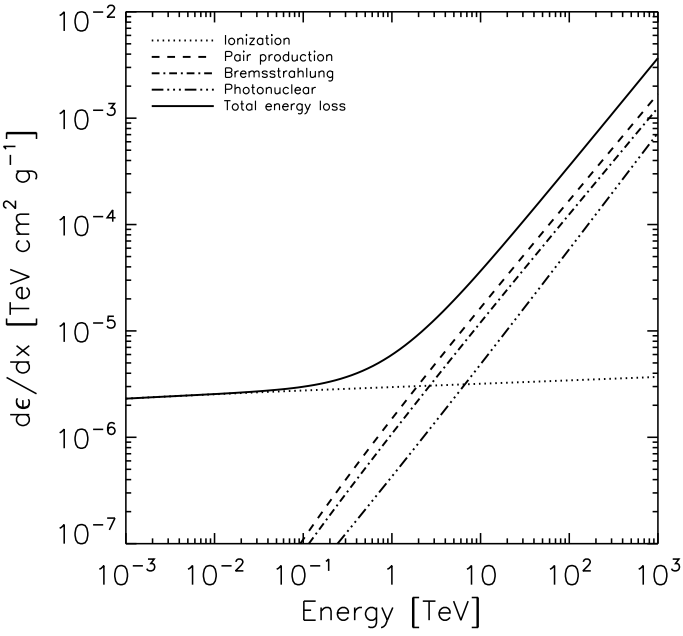

Figure 3.4: The muon energy loss in seawater as a function of energy, calculated from Equations 3.32 to 3.34. The total energy loss (solid line) is decomposed into contributions from different processes, indicated in the legend. This Figure is made using the values of Klimushin, Bugaev & Sokalski (2001).

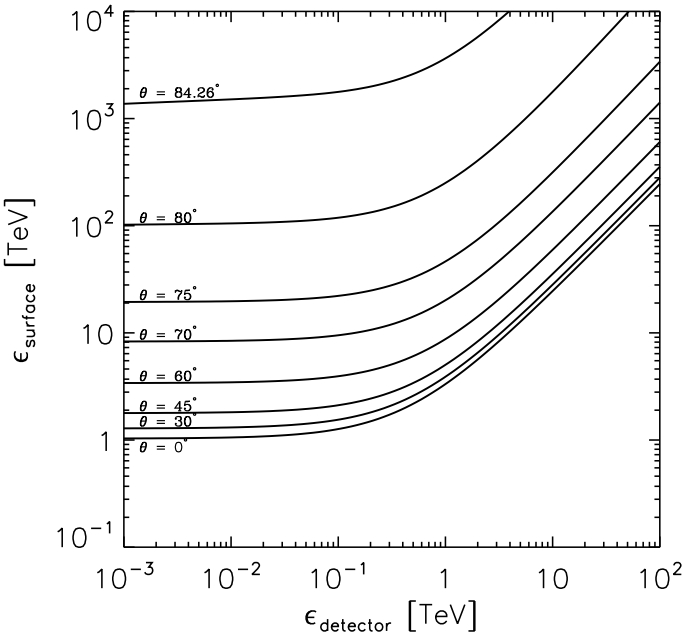

Figure 3.5: The muon energy loss by passing a layer of sea water with vertical depth $d = 2475$ m is pictured here in the form of muon energy at the surface of the sea $\epsilon_{\text{surface}}$ as a function of muon energy at the detector level $\epsilon_{\text{detector}}$. We plot the energy loss for different zenith distance θ, thus the path length is $R = d/\cos\theta$.

If we integrate Equation 3.31 we can obtain the integral equation

$$\int_{\epsilon_{\text{surface}}}^{\epsilon_{\text{detector}}} \frac{d\epsilon}{a(\epsilon) + b(\epsilon)\epsilon} + R = 0, \tag{3.35}$$

in which $\epsilon_{\text{surface}}$ is the energy at the surface of the sea and $\epsilon_{\text{detector}}$ is the energy at detector level, located at slant depth $R = d/\cos\theta$ where d is the vertical distance of the detector and θ is the zenith distance from which the source came. The slant depth formula assumes a plane-parallel layers of the sea which does not take into account the curvature of the Earth. This is however a good approximation for zenith distances less than $\sim 85^\circ$, which is the range of zenith distances we are interested in.

Solving Equation 3.35, we can obtain $\epsilon_{\text{surface}}$ if $\epsilon_{\text{detector}}$ is the input and vice versa. I solve Equation 3.35 to obtain $\epsilon_{\text{surface}}$ as a function of $\epsilon_{\text{detector}}$. The result for ANTARES depth of $d = 2475$ m below sea level is shown in Figure 3.5 for several slant depths.

The relation between $\epsilon_{\text{surface}}$ as a function of $\epsilon_{\text{detector}}$ is particularly useful to obtain the muon flux at detector level:

$$\frac{dN}{d\epsilon_{\text{det}}}(\epsilon_{\text{det}}, R) = \frac{dN}{d\epsilon_{\text{sur}}}(\epsilon_{\text{sur}}) \left.\frac{d\epsilon_{\text{sur}}}{d\epsilon_{\text{det}}}\right|_{\epsilon_{\text{det}}, R} \tag{3.36}$$

With these in mind, we can now proceed to calculate the muon spectrum of a GRB based on its observed photon spectrum at the top of the atmosphere.

3.7 *On the multiplicity of downgoing muons*

THE CALCULATIONS of muon production developed in this Chapter is a time-averaged model and thus is incapable of predicting the rate of muon bundles due to the occurence of several muons produced in a γ-induced shower. It is important, however, to quantify accurately the rate of downgoing muon bundles, as they can be misidentified as signals expected from γ-induced muons.

To this end, simulations of muon production from γ showers have been performed with `CORSIKA` (Heck et al., 1998), a program built to simulate in detail extensive air showers initiated by cosmic-ray particles, including high-energy photons. A number of showers with primary photons ranging from 1 TeV to 100 TeV

ϵ_γ	N_γ	N_μ	$N_\mu(\epsilon_\mu \geq 0.7$ TeV)	$N_\mu(\epsilon_\mu \geq 0.9$ TeV)
1	1×10^7	1 647 016	223 (0.014%)	55 (0.003%)
2	1×10^7	3 652 709	1271 (0.035%)	772 (0.021%)
5	1×10^7	10 389 534	3924 (0.038%)	2573 (0.025%)
10	4×10^6	9 119 416	3515 (0.039%)	2228 (0.024%)
50	2×10^6	28 121 835	9802 (0.035%)	6420 (0.023%)
100	6×10^5	18 345 064	6016 (0.033%)	3960 (0.022%)

Table 3.1: A summary of the γ-induced electromagnetic shower simulations performed with CORSIKA. All simulations are performed with zenith distance $\theta = 30°$. Each row summarises the simulation results for photons with a given primary energy ϵ_γ. N_γ is the number of showers simulated; N_μ is the total number of muons produced from all simulations; $N_\mu(\epsilon_\mu \geq 0.7$ TeV) and $N_\mu(\epsilon_\mu \geq 0.9$ TeV) are the total number of muons with energies greater or equal than respectively 0.7 TeV and 0.9 TeV.

is produced (see Table 3.1 for details on the number of showers produced for each energy of the primary photon). Hadronic interactions in the atmosphere are simulated with the QGSJET model while the electromagnetic interactions are simulated with the EGS4 package. The photon source is fixed to an assumed position in the sky, with an azimuth angle of 0° (toward the North) and zenith distance of 30°.

The result of the simulation can be seen in Table 3.2 and Figure 3.6. Table 3.2 shows the rate of single muon events produced in each photon shower with given photon energy ϵ_γ. For each primary energies, single muon rates are shown for three different muon energy threshold: No threshold at all, $\epsilon_\mu \geq 0.7$ TeV, and $\epsilon_\mu \geq 0.9$ TeV. For each threshold, two quantities are shown: The number of showers that produce at least one muon passing the energy threshold and the number of shower producing only single muons passing the energy threshold.

Figure 3.6 shows the distribution of the muon multiplicity. For each shower with given photon energy ϵ_γ the distribution of the

Table 3.2: The rate of single muons for each shower with given primary energy ϵ_γ. For each given threshold energy, two quantities are shown: The number of showers that produce at least one muon with energy equal or larger than the given threshold and the number of showers that produce only one muon passing the given energy threshold.

ϵ_γ [TeV]	No threshold			$\epsilon_\mu \geq 0.7$ TeV			$\epsilon_\mu \geq 0.9$ TeV		
1	792740	529689	(66.82%)	208	208	(100.00%)	55	55	(100.00%)
2	945618	604308	(63.91%)	699	630	(90.13%)	435	415	(95.40%)
5	2181219	1203441	(55.17%)	2135	1914	(89.65%)	1365	1194	(87.47%)
10	1218344	511458	(41.98%)	1602	1409	(87.95%)	1020	905	(88.73%)
50	993949	21334	(2.15%)	3990	3207	(80.38%)	2746	2287	(83.28%)
100	599983	121	(0.02%)	4698	3652	(77.74%)	3215	2559	(79.60%)

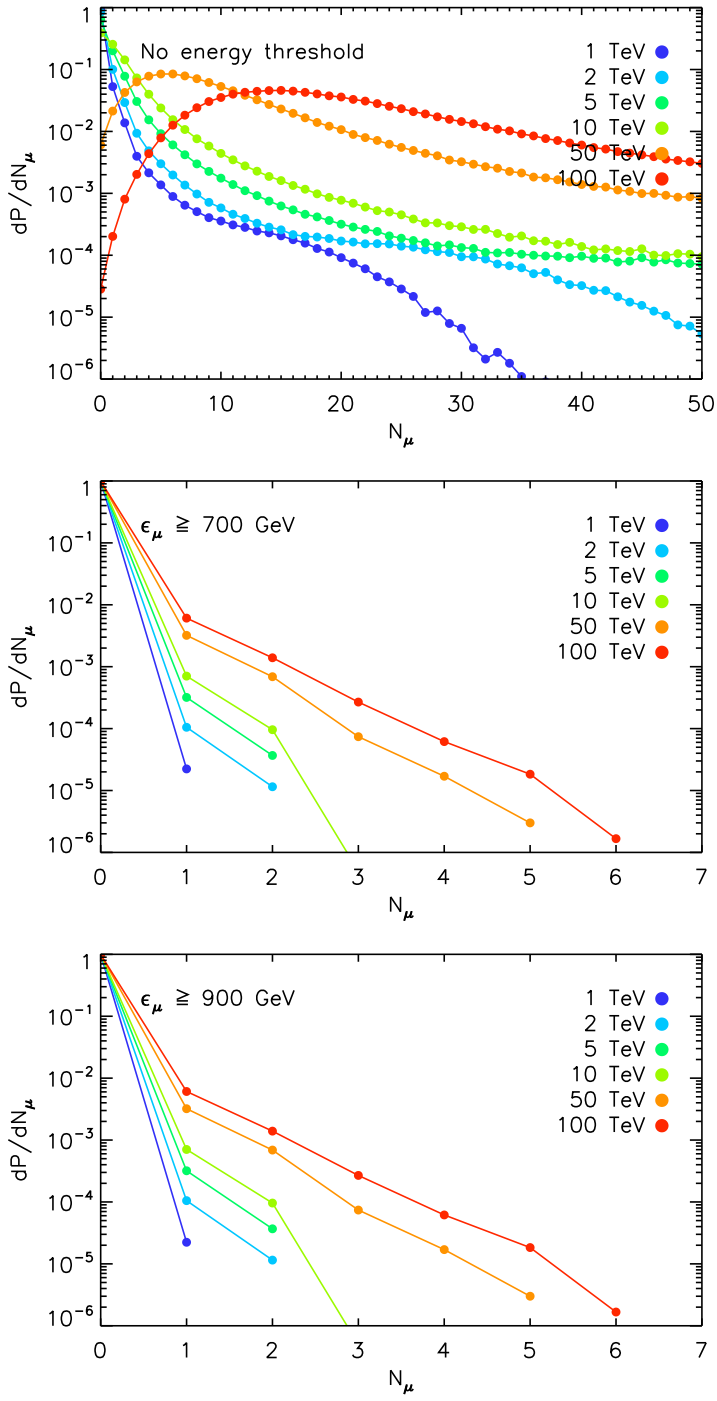

Figure 3.6: The distribution of muon multiplicity N_μ at the surface of the sea. Each curve shows the fraction of N_μ produced from showers with given photon-primary with energy ϵ_γ. Photons with energy $\epsilon_\gamma \gtrsim 10$ TeV can produce large muon bundles. However, if a certain muon energy threshold is applied (middle and bottom plots), we can see that the majority of the events are single muons.

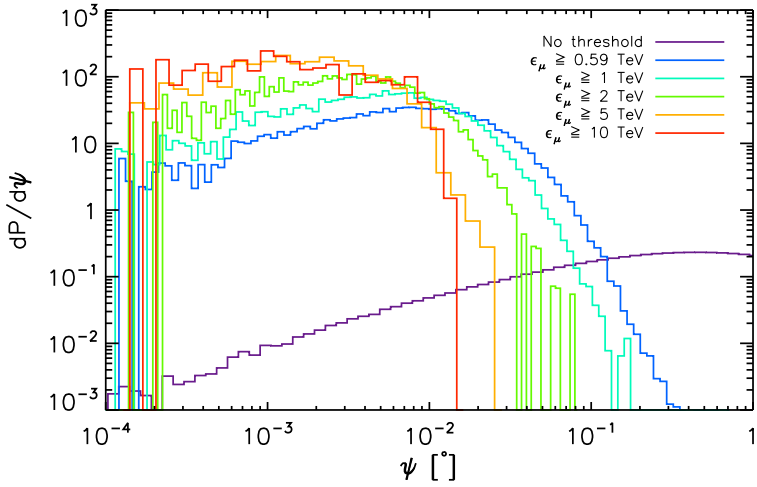

Figure 3.7: The distribution of the angular separation ψ of the original TeV photon track and the track of muons produced in the atmosphere. In addition to the distribution of ψ for all muons, the ψ distribution for six different muon energy thresholds are also shown. We can see that for TeV muons, the angular separations with the original photon tracks are very small they are practically parallel with them.

number of muons N_μ produced in the shower, at the surface of the sea, is shown. The top plot shows the distribution of N_μ for muons with any energy. We can see that for photon primaries with energy $\epsilon_\gamma \lesssim 10$ TeV, the majority of the showers produce no muons at all, with a probability of $\sim 20\%$ producing at least one muon. At higher primary energies, there is a higher chance to produce multiple muons within a shower. However, the muons must penetrate the depth of the sea in order to be detected by the ANTARES telescope. Thus only muons with sufficiently high energy are detected. If we only count muons with energy larger than 700 GeV (middle plot of Figure 3.6) or 900 GeV (bottom plot of Figure 3.6), it is clear that the majority of events contain a single muons and that high-energy muon bundles are rare. Table 3.2 shows that in the photon energy range of 2 TeV $\leq \epsilon_\gamma \leq$ 10 TeV, at most $\sim$11% of the muons with $\epsilon_\mu \geq 0.9$ TeV arrive in bundles. The rate of muon bundles is thus rather low.

If the very high energy muon bundles pass through the detector, it is still possible to reconstruct a track. At this energy, the muons will travel essentially at parallel angles and could therefore be reconstructed as a single muon track. This is due to the limited two-track resolution of the detector that hinders the abil-

ity to distinguish multiple muon tracks coming at approximately the same time (Halzen, Kappes & Ó Murchadha, 2009). From the CORSIKA simulation, we could calculate the angular separation ψ of the tracks with respect to the original photon directions. In Figure 3.7 the distribution of ψ is plotted for muons with any energy as well as for muons passing a certain energy threshold. Six energy thresholds are considered, ranging from 590 GeV to 10 TeV. We can see that for TeV muons, the distribution of ψ is peaked at around $\sim 0.001^\circ$, which is much smaller than the angular resolution of the ANTARES detector.

Consequently, the simulations of ANTARES' sensitivity to downgoing muons can then be performed by generating single muon tracks. We will discuss this simulation in Chapter 7.